Plasmonics Under the Infrared Microscope: *Sensing and Spectra of Single Particles Using Metal Film Hole Arrays*

Marvin A. Malone, Katherine E. Cilwa, Antriksh Luthra, Matthew McCormack, David Lioi, and James V. Coe*
The Ohio State University Department of Chemistry
100 West 18th Avenue
Columbus OH 43210-1173, USA
coe.1@osu.edu

***Abstract*—Measurements and modeling of plasmonic resonance positions as a function of orientation are presented in a manner that connects the common geometries with a formalism for all of momentum space. This framework is useful for understanding dispersion studied under an infrared microscope by rotating the sample about the optical axis of the microscope. Applications using the microscope for sensing and spectra of individual particles are presented.**

Keywords: plasmonics, surface plasmon polaritons, metal films with hole arrays, single particle sensing and spectra

I. Introduction

This work demonstrates how plasmonic studies on metal films with square arrays of holes (mesh) can be pursued under a microscope. It is interesting to consider how our understanding of the plasmonics changes from a well-understood semi-infinite film to individual microscopic particles. Since the microscope utilizes a wide range of angles and it is desirable to keep the plasmonic system within the microscope's focal plane, there are significant geometric changes that must be considered in pursuing plasmonic dispersion under a microscope.

A unified approach to dispersion diagrams for plasmonic resonances is presented that links standard dispersion measurements in the typical symmetries of square lattices (ΓX and ΓM as explored by rotating mesh about an axis within the mesh)[1-10] to dispersion by rotation of the mesh in the focal plane of a microscope (rotation about the optical axis of the microscope). This approach essentially covers all of momentum space including some less-explored regions of the momentum space of square metal lattices. The work is illustrated with data from metal film hole arrays that exhibit plasmonic transmission resonances in the infrared (IR) regime[10, 11].

There have been a number of reviews on metal film arrays[12-17]. Under certain conditions, light incident upon a metal mesh can be made to run along the front and back surfaces of the mesh. Briefly, there exist wavelengths at which diffraction spots are no longer transmitted by the mesh, i.e. the light is bent parallel to the surface (in fact resonances are labeled by the diffraction spots that are no longer transmitted)[18]. Light running along the surface of the metal interacts with conducting electrons in the metal producing surface plasmon polaritons (SPPs), mixed states between light and waves of conducting electrons. When SPPs come to a hole, light can be coupled back out without being scattered from the incident beam. We think of the mesh as an inside out fiber optic[19]. As a result, the light is made to sample subwavelength spaces like the holes in the mesh, which turns out to be useful for taking scatter-free spectra of individual, subwavelength-sized particles[20-22]. We will also show how the addition of an aperture to an IR microscope system allows the observation of narrow plasmonic resonances in spite of the large range of angles employed by a microscope. This adaptation is used to sense individual particles by the shift of resonances.

The mesh used in these studies was obtained from Precision Eforming of Cortland, NY (www.precisioneforming.com). It is nickel with a square lattice of square holes (5.4 µm wide square holes, 12.6 µm lattice parameter, and a thickness of ~2 µm). A scanning electron microscope image is given in Fig. 1.

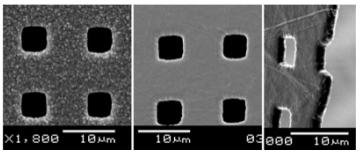

Figure 1. Scanning electron microscope image of the mesh used in these experiments. Front, back, and side views of the nickel mesh. The white bar is 10 µm.

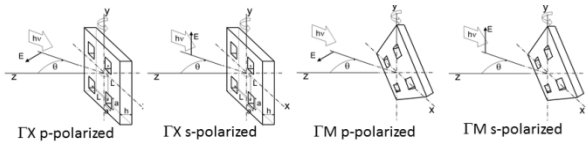

Figure 2. Common geometries for observing the dispersion of transmission resonances of a square lattice of holes in a metal film including polarization of the incident light.

II. ΓX and ΓM Dispersion

The standard geometries involved with directing light at a mesh are defined in Fig. 2. In this work, the light is perpendicularly incident upon the mesh along the *z*-axis and the *x*- and *y*- directions are along the surface of the mesh. Let rotation about the *x*, *y*, and *z*-axes be defined by the γ, θ, and ϕ

978-1-4577-0911-1/12/$31.00 ©2012 IEEE

angles, respectively. With the arrangements of Fig. 2, dispersion for both the ΓX and ΓM geometries is assayed by recording spectra as θ (rotation about the y-axis within the mesh) is varied. The ΓX orientation has ϕ=0° (rotation about the z-axis) and the ΓM orientation has ϕ=45°, while both have γ=0°. Allowing for manipulations of only θ and ϕ (not γ), the momentum wavevectors parallel to the mesh surface are given generally as

$$k_x = 2\pi\tilde{\nu}sin\theta cos\varphi, \quad (1)$$

$$k_y = 2\pi\tilde{\nu}sin\theta sin\varphi, \quad (2)$$

where $\tilde{\nu}$ is the wavenumber (reciprocal of the wavelength). In order to better connect with the microscope geometry which follows, the wavevector parallel to the surface is taken as k_x+k_y, which simplifies in the ΓX and ΓM geometries.

Extensive details of the data acquisition have been provided elsewhere[10]. The FTIR spectra were obtained with a Perkin Elmer Spectrum GX instrument. Spectra were measured with 8 cm^{-1} resolution, averaging 50 scans each, within a range of 500-4000 cm^{-1}, and varying θ in steps of one degree from -5° to 50° for both the ΓX and ΓM orientations. Peak centers were obtained by interpolation using the instrument's software. The data are shown in Fig. 3 using closed red circles for the p-polarized data (electric-field of the light parallel with the x-axis) and closed blue symbols for the s-polarized data (electric-field of the light parallel with the y-axis).

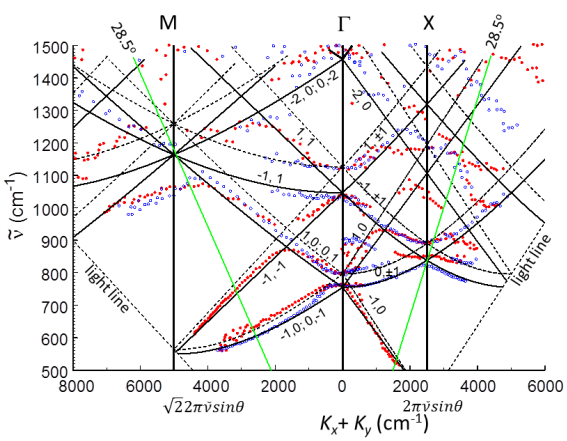

Figure 3. An unfolded dispersion diagram of measured resonance positions (symbols) in the ΓX (right) and ΓM (left) geometries. The light line and its folded analogs are shown with dotted black lines. The black solid curves are momentum matching curves described in the text. The ½ Brillouin zones are indicated with vertical black lines. The green solid lines correspond to θ being fixed at 28.5° which connects to the following microscope study.

Momentum matching equations were derived in terms of the variable angle, θ. It is important to allow the effective index of refraction of mesh to vary with wavelength

$$n_{eff}(\tilde{\nu}) = \alpha_0 + \frac{\alpha_1}{\tilde{\nu}} \quad . \quad (1)$$

This choice means that $n_{eff}(\tilde{\nu})$ will not be valid outside of the modeled range, but it permits the dispersion equation to be solved as a quadratic. Values of α_0=1.134 and α_1= -59.94 were used to model the data. This gives a value of n_{eff}=1.055 @ 760 cm^{-1} and n_{eff}=1.080 @ 1100 cm^{-1}. Letting i, j identify a resonance and using L as the lattice parameter, then the position of a resonance in the ΓX orientation is

$$\tilde{\nu}_{\Gamma X}(i,j,\theta) = \frac{\frac{2isin\theta}{L} - 2\alpha_0\alpha_1 + \sqrt{\left(2\alpha_0\alpha_1 - \frac{2isin\theta}{L}\right)^2 - 4(\alpha_0^2 - sin^2\theta)\left(\alpha_1^2 - \frac{i^2+j^2}{L^2}\right)}}{2(\alpha_0^2 - sin^2\theta)} \quad (2)$$

Likewise, the position of a resonance in the ΓM orientation is

$$\tilde{\nu}_{\Gamma M}(i,j,\theta) = \frac{\sqrt{2}(i+j)sin\theta/L - 2\alpha_0\alpha_1 + \sqrt{\left(2\alpha_0\alpha_1 - \frac{\sqrt{2}(i+j)sin\theta}{L}\right)^2 - 4(\alpha_0^2 - sin^2\theta)(\alpha_1^2 - (i^2+j^2)/L^2)}}{2(\alpha_0^2 - sin^2\theta)} \quad (3)$$

The wavevector on the independent axis of Fig. 3 is k_x+k_y, however this simplifies to $2\pi\tilde{\nu}sin\theta$ in the ΓX geometry (ϕ=0°) and to $\sqrt{2}2\pi\tilde{\nu}sin\theta$ in the ΓM geometry (ϕ=45°). Bandgaps are particularly evident at the Γ point at $\tilde{\nu}$ =750 cm^{-1} and $\tilde{\nu}$ =1100 cm^{-1}, and at k_x+k_y=2500 cm^{-1} in ΓX space at $\tilde{\nu}$ =850 cm^{-1}, which show the strong interactions of light that is trapped at the surface of a metal mesh in the form of a polariton. There are also some very interesting polarization features. In ΓX space, the 1,0 and -1,0 features are p-polarized and similar to those of one-dimensional gratings[23, 24], but the 0,±1 feature is s-polarized (characteristic of bigratings) and strongly split (it is expected to be one resonance). In ΓM space, the -1,0 and 0,-1 features are also expected to be degenerate, but they are split into separate s- and p-polarized trends. In ΓX space, the crossing of the -1,±1 and 0,±1 resonances gives a band gap that splits into three groups: the lowest is p-polarized, the middle is s-polarized, and the top has both polarizations.

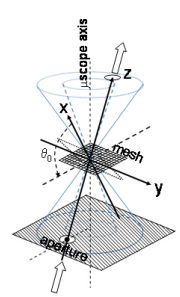

Figure 4. An aperture is added to the Cassegrain optical system of an IR microscope in order to narrow the plasmonic transmission resonances. The aperture is added off of the optical axis and 25 mm below the focal plane of the microscope. The system is positioned so that the mesh can be rotated about the optical axis of the microscope in order to disperse the resonances. If considered in terms of the arrangements in Fig. 1, then θ has been fixed (at ~28.5°) and dispersion is studied by varying ϕ.

III. Φ Dispersion Under the Microscope

Our Perkin Elmer Spotlight 300 IR microscope focuses a ring of light (from 17° to 37° off of the optical axis) onto the sample and then collects a similar ring of light from the sample, i.e. no light goes perpendicularly through the sample and a large range of angles is presented to the sample, as pictured in

Fig. 4. This arrangement produces dispersion which spreads out the narrow resonances that are observed in the ΓX and ΓM geometries. The microscope spectrum of mesh produces a good detector curve for taking spectra of microscopic particles (as will be shown in a later section), but this is bad for sensing which works better with narrow resonances. An IR microscope can be turned into a plasmonic sensor by the simple addition of an aperture[11]. The geometry is pictured in Fig. 4. A 2.4 mm diameter aperture was placed 13.9 mm off of the optical axis (keeping y=0) and ~24 mm below the focal plane of the IR microscope. Dispersion is studied by rotating the mesh about the optical axis of the microscope, i.e. by varying ϕ and fixing θ at θ_0=28.5°. Details about the collection of data have been given previously[11]. In the previous work, the data were plotted against ϕ, but in this work, the data is plotted against k_x+k_y , as given below

$$k_x + k_y = 2\pi\tilde{\nu} sin\theta_0(cos\varphi + sin\varphi). \quad (4)$$

The data (black filled circles) are presented in Fig. 5. The experimental data were measured in the region of ϕ=0-90° and have been projected to the region of ϕ=90-180° (open circles).

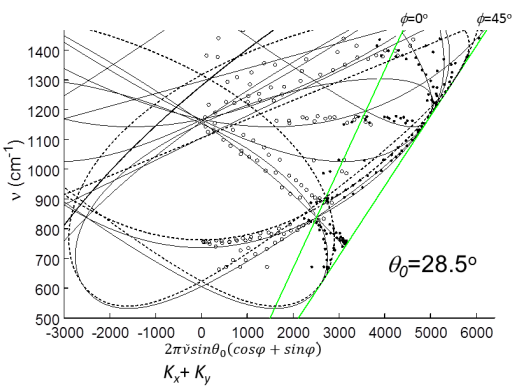

Figure 5. Dispersion diagram of transmission resonances observed (black circles) in an IR microscope with an aperture by rotating mesh about the optical axis of the microscope. The open circles are a projection of experiement into the ϕ=90-180° region. The green solid lines are slices that connect with the green lines shown in Fig. 2. The black dotted lines correspond to the folding of the light line into this wavevector space (not all are shown). The solid black lines are momentum matching dispersion curves given in eq. (5) using the same values of n_{eff} as used in the ΓX and ΓM work.

Momentum matching equations give the position of a resonance in ϕ-space as

$$\tilde{\nu}_\varphi(i,j,\varphi) = \frac{\left\{2sin\theta_0(icos\varphi+jsin\varphi)/L-2\alpha_0\alpha_1+\sqrt{(2\alpha_0\alpha_1-2sin\theta_0(icos\varphi+jsin\varphi)/L)^2-4(\alpha_0^2-sin^2\theta_0)(\alpha_1^2-(i^2+j^2)/L^2)}\right\}}{2(\alpha_0^2-sin^2\theta_0)}. \quad (5)$$

While θ has been fixed to model our microscope geometry, note that the use of variable values of θ in eq. (5) effectively covers all of momentum space. There can be surprises in exploring the rest of momentum space. Due to the symmetry of a square lattice mesh, the primary resonances at the Γ point correspond to wavelengths at which four diffraction spots are no longer transmitted becoming evanescent waves. However, the tilting of a mesh by θ_0=28.5° (specific value depends on n_{eff}) and ϕ=45° puts the mesh in a position where 8 different diffraction spots are no longer transmitted simultaneously becoming evanescent waves.

IV. Sensing Single Particles Under the IR Microscope

Using the aperture modification, the -1,-1 resonance (with ϕ=45° occurring at ~750 cm^{-1}[11]) was observed to be very narrow (~20 cm^{-1}) which is good for sensing. It was tested by sensing polystyrene (latex) microspheres. Previously, we have used latex microspheres to measure the propagation distance of IR light along the surface of the mesh[25]. The latex microspheres were 5.0 ± 0.4 μm in diameter, which nicely matches the holes of the plasmonic mesh. They were obtained from SPI Supplies (P.O. Box 656, West Chester, PA, 19381-0656, www.2spi.com, Product no. 02705, Lot no. 1120920) and have a refractive index at 1.58 @ 540 nm. They come in an aqueous colloidal suspension and a drop was applied to the mesh. As the drop spreads, solution gathers in the holes and capillary action pulls many spheres into the holes. After washing and drying, transmission spectra were recorded in regions containing from 0 to 5 microspheres within a 150 μm by 150 μm window (shown as pink squares on the top and right sides of Fig. 5). The spectra were recorded in point mode with a Perkin Elmer Spotlight 300 instrument using 50 scans, 4 cm^{-1} resolution, a range of 600-4000 cm^{-1}, and a liquid nitrogen cooled MCT detector. Spectra in the region of the -1,-1 resonance are shown at the bottom left of Fig. 5.

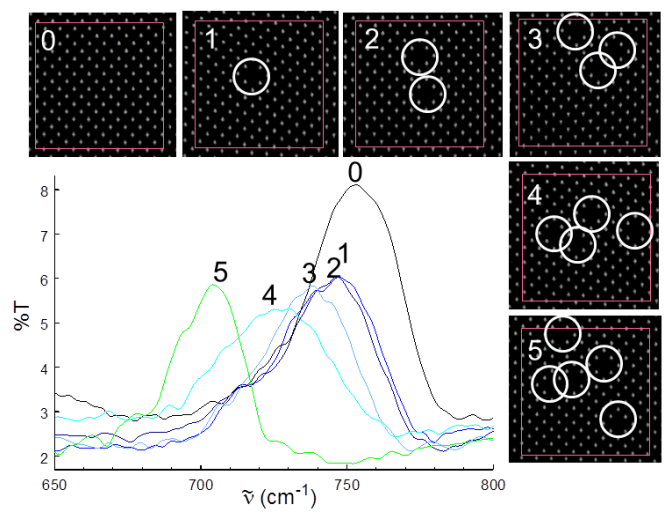

Figure 5. Top and right are microscope optical images of mesh with different number of latex spheres caught in the holes. The windows of 150 µm by 150 µm are shown with pink rectangles. Each white spot is a microchannel and filled holes are dark under these conditions. At the bottom left are transmission spectra (using an aperture with the IR microscope) of the -1,-1 resonance with ϕ=45° for each different number of microspheres in the window.

The -1,-1 resonance shifts to lower frequency with a larger number of microspheres. The shifts get increasingly larger. Noting that the window contains 142 holes, a plot of the resonance position vs the fraction of holes filled with microspheres is presented in Fig. 6. A nonlinear least squares

fit was performed using a logistic sigmoid function for the resonance position

$$\tilde{\nu} = \frac{\tilde{\nu}_0 - \tilde{\nu}_{FC}}{1+\left(\frac{f}{b}\right)^P} + \tilde{\nu}_{FC}, \qquad (6)$$

where $\tilde{\nu}_0$ is the position with no holes filled, $\tilde{\nu}_{FC}$ is the position with all holes filled (full coverage), f is the fraction of holes filled (independent variable), b is the fraction of maximum sensitivity at the inflection, and P sets the slope at the inflection. The fitted line in Fig. 6 has $\tilde{\nu}_0$=749.3±2.3 cm^{-1}, b=0.046±0.003, and P=3.8±0.8 with $\tilde{\nu}_{FC}$ fixed at 585 cm^{-1}. While more data is needed with a larger number of microspheres within the window in order to know if this functional form is correct, it is very interesting that this fitted function predicts maximum sensitivity when f=b, i.e. at a fraction corresponding to only 6.5 microspheres. This plasmonic resonance is good for detecting or sensing the number of microspheres in the lower range of the fraction filled.

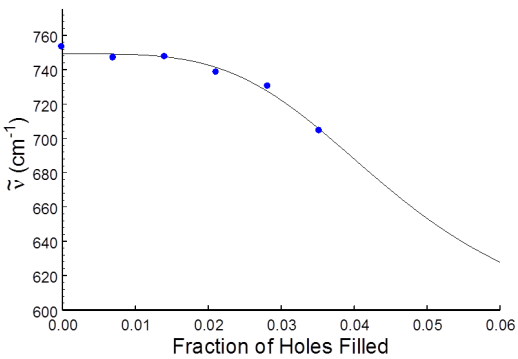

Figure 6. Shift of the -1,-1 resonance with ϕ=45^0 for each different number of microspheres in the window. The data were fit to eq. (6) giving the solid black curve.

V. Spectra of a Single Particle Under the IR Microscope

The extinction spectra of a latex microsphere on a ZnSe window and the absorption spectra of a latex microsphere in mesh were recorded using a Perkin Elmer Spectrum Spotlight 300 FTIR imaging microscope, equipped with 16 liquid-nitrogen-cooled, mercury-cadmium-telluride (MCT) detectors. The microspheres were from the same sample described above. In imaging mode, spectra are recorded at each pixel on a 6.25 µm square grid within an image area defined by the user. For this experiment, a 3 pixel by 3 pixel box was used (18.75 µm x 18.75 µm) which had been previously calibrated and acts like a 19.3 µm x 19.3 µm window[22, 26]. Spectra were recorded at 4 cm^{-1} resolution using 256 scans per pixel for microspheres on ZnSe and 512 scans per pixel for microspheres in mesh holes. The average extinction spectrum of 16 different polystyrene microspheres on ZnSe is presented in Fig. 7. The 5 µm diameter of the microsphere corresponds to a wavelength at 2000 cm^{-1} and a large broad peak is observed in this region as predicted by Mie theory[27]. Particles of similar size to the wavelength are known to efficiently scatter light[27, 28]. Vibrational features are evident, but an order of magnitude smaller than the scattering. They exhibit distorted lineshapes, i.e. the Christensen effect[29]. The average absorption spectrum of 19 polystyrene microspheres in mesh, is presented in Fig. 8. Notice that the vibrational features are now dominant and observed in the normal phase of absorption. This spectrum is free of the typical Mie scattering effects associated with particles of size similar to the wavelength.

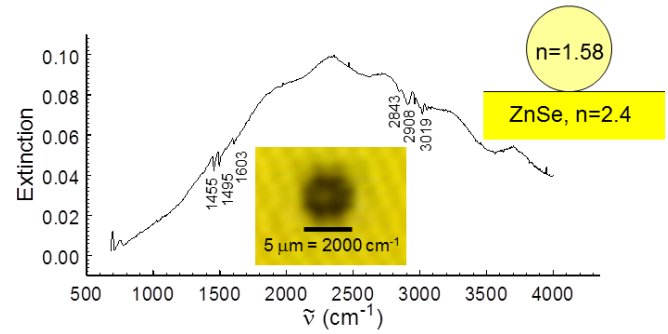

Figure 7. The average extinction spectrum of 16 different, 5 µm diameter, latex microspheres as obtained with an effective window of 19.3 µm x 19.3 µm. A schematic of the system is inset at the upper right. An experimental optical image of a single microsphere on ZnSe is inset below the extinction curve.

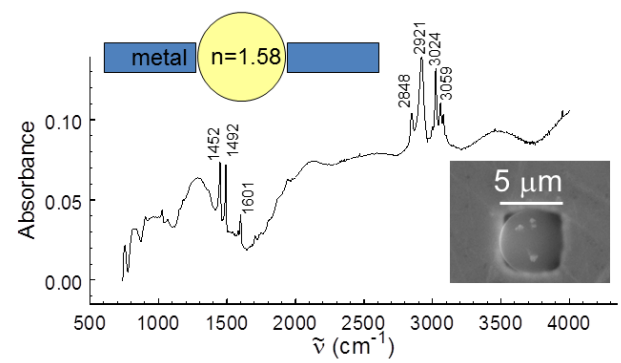

Figure 8. The average absorption spectrum of 19 different, individual, 5 µm diameter, latex microspheres in mesh holes as obtained with an effective window of 19.3 µm x 19.3 µm. A schematic of the system is inset at the upper left. A scanning electron microscope image of a single microsphere in a mesh hole is inset at the lower right.

The spectra of Figs. 7 and 8 were modeled using Mie theory taking Fig. 7 as extinction and Fig. 8 as absorption. Scaling factors and offsets were employed to place these spectra on the same absolute scale using common vibrational parameters as a constraint. A polystyrene microsphere, being both spherical and homogeneous, is an excellent Mie particle. The extinction spectrum of polystyrene on ZnSe was modeled using a Mie expression for the absolute extinction cross section

$$C_{ext} = \frac{1}{2\pi\tilde{\nu}^2}\sum_{n=1}^{\infty}(2n+1)\Re(a_n + b_n), \qquad (7)$$

where a_n and b_n are the well-known Mie coefficients which are functions of r, the radius of the particle and m, the complex refractive index of the particle. The complex refractive index can be written in terms of the complex dielectric, ε, and the vibrations of the material as

$$m^* = \sqrt{\varepsilon} = \sqrt{\varepsilon' + \varepsilon'' + \sum_j \frac{A_j \tilde{\nu}_{0j}^2}{\tilde{\nu}_{0j}^2 - \tilde{\nu}^2 - i\gamma_j \tilde{\nu}}}, \quad (8)$$

where m^* is the complex conjugate of m, ε' and ε'' are the real and imaginary constant parts of ε respectively, and j is an index for a sum over vibrations (A_j is the strength, $\tilde{\nu}_{0j}$ is the position, and γ_j is the full width at half maximum of each vibration). The extinction spectrum on ZnSe was offset by 0.004 and multiplied by 7.511×10^{-6} (top solid curve) to match the Mie theory prediction (dotted curve, r=2.36 µm, ε' = 2.56, and ε'' = 0.040) as shown in Fig. 9. The scattering cross section is

$$C_{scat} = \frac{1}{2\pi\tilde{\nu}^2} \sum_{n=1}^{\infty} (2n+1)[|a_n|^2 + |b_n|^2], \quad (9)$$

where the absorption cross section is C_{abs}=C_{ext}-C_{scat}. The spectrum of Fig. 8 was offset of 0.040 and multiplied by $(7.511 \times 10^{-6})/5.0$ to get the absorption curve at the bottom of Fig. 9. Since extinction is the sum of scattering and absorption contributions, the scattering curves were obtained by subtracting the absorption from the extinction. Clearly, scattering is the dominant component with latex microspheres. The vibrational parameters of Table 1 were adjusted until they matched the experimental plots in extinction, scattering, and absorption in Fig. 9. The vibrations of polystyrene are fairly narrow and weak compared to the scattering, so the mutual agreement of these different experiments as placed on an absolute scale gives more confidence to the vibrationally modified dielectric function of eq. (8) and the values in Table 1 which also serve as a determination of the absolute phonon transition strengths.

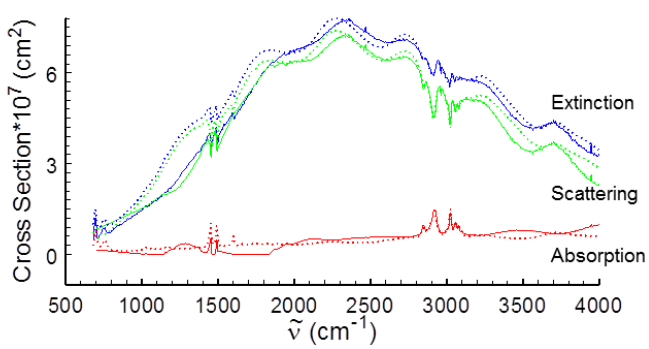

Figure 9. The extinction spectrum of Fig. 7 and absorption spectrum of Fig. 8 were scaled so as to consistently fit on an absolute scale with a common set of vibrational parameters for the polystyrene microspheres. The Mie theory predictions are given with dotted traces, while the scaled experimental work is presented with solid traces.

VI. Conclusion

The dispersion behavior of plasmonic metal mesh under the IR microscope as modified with an aperture has been observed by rotating the mesh about the optical axis of the microscope (variation of ϕ with a fixed value of θ_0). The dispersion behavior has been shown to be consistent with more conventional studies in the standard ΓX and ΓM geometries. The green lines in Fig. 3 for ΓX and ΓM correspond to the green lines in Fig. 5 for the microscope and ϕ-space (rotation about the microscope's optical axis). The use of an aperture with the IR microscope has enabled the observation of a narrow transmission resonance (-1,-1 with ϕ=45°). Increasingly large shifts of this resonance have been observed with increasing numbers of microspheres within the holes of the mesh showing that sensing experiments are possible with an imaging IR microscope system. Furthermore, the IR microscope system (without an aperture) has been shown to produce scatter-free, IR absorption spectra of single particles for which much of the spectrum has longer wavelengths than the size of the particle. Together these results successfully demonstrate that both sensing and spectroscopy can be performed on single particles with an imaging IR microscope. Future work will establish how sensing works with individual microscopic particles in contrast to the well-understood behavior of films on semi-infinite metals.

Table 1. Vibrational parameters of polystyrene [eq. (8)].

A_j	$\tilde{\nu}_{0j}(cm^{-1})$	$\gamma_j(cm^{-1})$
0.00009	3102	19
0.0002	3080	17
0.0003	3058	18
0.0006	3024	15
0.00012	2998	15
0.0017	2916	38
0.00037	2848	30
0.00005	1961	30
0.0001	1943	30
0.00005	1890	30
0.0001	1871	30
0.00005	1821	30
0.0001	1805	30
0.00005	1746	30
0.0001	1736	30
0.00005	1677	30
0.0001	1660	30
0.00045	1600	12
0.0001	1582	12
0.0001	1553	30
0.00005	1542	30
0.0012	1491	10
0.0013	1451	10
0.0005	1441	13
0.00015	1373	30
0.00007	1182	12
0.00012	1154	12
0.0003	1068	20
0.0005	1028	20
0.007	757	35
0.003	748	35
0.015	696	20

ACKNOWLEDGMENT

We thank the USA National Science Foundation for support of this work under grant numbers CHE 0848486 and CHE-0639163.

REFERENCES

1. Williams, S.M., *Characteristics and Applications of the Infrared Enhanced Transmission of Metallic Subwavelength Arrays*, in *Chemistry*. 2006, The Ohio State University: Columbus OH. p. 405.
2. Tsai, M.-W., et al., *Dispersion of surface plasmon polaritons on silver film with rectangular hole arrays in a square lattice.* Applied Physics Letters, 2006. **89**(9): p. 093102/1-093102/3.
3. Tsai, M.-W., et al., *Bragg scattering of surface plasmon polaritons on extraordinary transmission through silver periodic perforated hole arrays.* Applied Physics Letters, 2006. **88**(21): p. 213112/1-213112/3.
4. Williams, S.M., et al., *Accessing surface plasmons with Ni microarrays for enhanced IR absorption by monolayers.* Journal Of Physical Chemistry B, 2003. **107**(43): p. 11871-11879.
5. Williams, S.M. and J.V. Coe, *Dispersion study of the infrared transmission resonances of freestanding Ni Microarrays.* Plasmonics, 2006. **1**(1): p. 87-93.
6. Ebbesen, T.W., et al., *Extraordinary optical transmission through sub-wavelength hole arrays.* Nature (London), 1998. **391**(6668): p. 667-669.
7. Ghaemi, H.F., et al., *Surface plasmons enhance optical transmission through subwavelength holes.* Physical Review B: Condensed Matter and Materials Physics, 1998. **58**(11): p. 6779-6782.
8. Barnes, W.L., et al., *Surface Plasmon Polaritons and Their Role in the Enhanced Transmission of Light through Periodic Arrays of Subwavelength Holes in a Metal Film.* Physical Review Letters, 2004. **92**(10): p. 107401-107401-4.
9. Williams, S.M., et al., *Extraordinary infrared transmission of Cu-coated arrays with subwavelength apertures: Hole size and the transition from surface plasmon to waveguide transmission.* Applied Physics Letters, 2004. **85**(9): p. 1472-1474.
10. Cilwa, K.E., *Surface Plasmon Polaritons and Single Dust Particles*, in *Chemistry*. 2011, The Ohio State University: Columbus.
11. Malone, M.A., et al., *Modifying an Infrared Microscope To Characterize Propagating Surface Plasmon Polariton-Mediated Resonances.* The Journal of Physical Chemistry C, 2011. **115**(25): p. 12250.
12. Sinton, D., R. Gordon, and A.G. Brolo, *Nanohole arrays in metal films as optofluidic elements: progress and potential.* Microfluidics and Nanofluidics, 2008. **4**(1-2): p. 107-116.
13. Gordon, R., et al., *Resonant optical transmission through hole-arrays in metal films: physics and applications.* Laser & Photonics Review, 2009.
14. Coe, J.V., et al., *Extraordinary transmission of metal films with arrays of subwavelength holes.* Annual Review Of Physical Chemistry, 2008. **59**: p. 179-202.
15. Coe, J.V., et al., *Metal films with Arrays of tiny holes: Spectroscopy with infrared plasmonic scaffolding.* Journal Of Physical Chemistry C, 2007. **111**(47): p. 17459-17472.
16. Brolo, A.G., et al., *Nanohole Arrays in Metal Films as Integrated Chemical Sensors and Biosensors Optical Guided-wave Chemical and Biosensors I*, O.S. Wolfbeis, Editor. 2009, Springer Berlin Heidelberg. p. 155.
17. Genet, C. and T.W. Ebbesen, *Light in Tiny Holes.* Nature (London, United Kingdom), 2007. **445**: p. 39-46.
18. Vigoureux, J.M., *Analysis of the Ebbesen experiment in the light of evanescent short range diffraction.* Optics Communications, 2001. **198**(4-6): p. 257-263.
19. Ulrich, R. and R.J. Martin, *Geometrical optics in thin film light guides.* Appl. Opt. FIELD Full Journal Title:Applied Optics, 1971. **10**(9): p. 2077-85.
20. Heer, J., et al., *Infrared Sensitivity of Plasmonic Metal Films with Hole Arrays to Microspheres In and Out of the Holes.* J. Phys. Chem. C, 2010. **114**: p. 520-525.
21. Cilwa, K.E., et al., *Scatter-Free IR Absorption Spectra of Individual, 3-5 μm, Airborne Dust Particles Using Plasmonic Metal Microarrays: A Library of 63 Spectra.* The Journal of Physical Chemistry C, 2011. **115**(34): p. 16910.
22. Malone, M.A., et al., *Modifying infrared scattering effects of single yeast cells with plasmonic metal mesh.* Journal of Chemical Physics, 2010. **133**(18): p. 185101.
23. Ritchie, R.H., et al., *Surface-plasmon resonance effect in grating diffraction.* Phys. Rev. Lett., 1968. **21**(22): p. 1530-3.
24. Schroter, U. and D. Heitmann, *Surface-plasmon-enhanced transmission through metallic gratings.* Physical Review B: Condensed Matter and Materials Physics, 1998. **58**(23): p. 15419-15421.
25. Cilwa, K.E., et al., *Propagation lengths of surface plasmon polaritons on metal films with arrays of subwavelength holes by infrared imaging spectroscopy.* Journal Of Chemical Physics, 2009. **131**(1): p. 061101.
26. Malone, M.A., *Infrared Microspectroscopy: A Study of the Single Isolated Bread Yeast Cell*, in *Chemistry*. 2010, The Ohio State University: Columbus.
27. van de Hulst, H.C., *Light scattering by small particles*. 1958, New York: John Wiley and Sons.
28. Bohren, C.F. and D.R. Huffman, *Absorption and Scattering of Light by Small Particles*. 2007: Wiley-VCH Verlag GmbH. 530.
29. Christiansen, C., *Untersuchungen über die optischen Eigenschaften von fein vertheilten Körpern.* Annalen der Physik, 1884. **259**(10): p. 298-306.